Available online at www.sciencedirect.com
SCIENCE DIRECT
Journal of Colloid and Interface Science 288 (2005) 562–569
JOURNAL OF Colloid and Interface Science
www.elsevier.com/locate/jcis

Simultaneous imbibition–heat convection process in a non-Darcian porous medium

M. Sánchez [a], E. Luna [a], A. Medina [a], F. Méndez [b,*]

[a] *Grupo de Medios Porosos y Granulados y PIMAC, IMP, 07730 México, DF, Mexico*
[b] *Facultad de Ingeniería, UNAM, 04510 México, DF, Mexico*

Received 15 December 2004; accepted 6 March 2005

Available online 16 April 2005

Abstract

In the present work, the nonisothermal imbibition process in a porous medium was numerically analyzed using a non-Darcian model for the momentum equation and energy equations for the wetting and dry zones. In order to show the thermal character of the problem, we assume initially that the porous medium is found at a uniform temperature T_0 and suddenly begins the imbibition process into the porous medium with a penetrating fluid at temperature T_1. The physical influence of nondimensional parameters such as Peclet number, Pe, effective heat capacity number, β_w, porous Reynolds number, $\mathrm{Re_p}$, and the inertial coefficient of the porous medium, F, serve us to evaluate the position and velocity of the imbibition front as well as temperature profiles in both zones. In particular, for values of $\mathrm{Re_p}F/\beta_w \gg 1$, we recover a type of nonisothermal Washburn law. The numerical predictions show that the imbibition front and the temperature fields strongly depend on the above nondimensional parameters, revealing a clear deviation of the simple Washburn law.

Keywords: Nonisothermal imbibition; Porous medium; Heat convective transport; Non-Darcian flow; Imbibition front

1. Introduction

The theoretical and experimental analysis of imbibition of a liquid—driven by surface tension—in a porous medium is a well-known phenomenon that makes it possible to explore several physical effects in capillary penetration dynamics. This simple situation of a liquid invading a porous medium has great importance in various technological applications: oil recovery, ink penetration in paper, fluid transport in plants or imbibition of water into seeds, transport of fluids in textile industry, capillary pumped loops, etc. Well-documented applications and fundamental aspects can be found elsewhere [1–4]. In general, we can identify the imbibition as a spontaneous process for which a wetting viscous fluid displaces or pushes aside a less no-wetting viscous one. Sometimes this action can only be sustained by capillary forces, with no external pressure. In this last case, we treat spontaneous imbibition. In the above discussion, we accept obviously that both fluids are immiscible. Therefore, in this class of theoretical and experimental studies the front of displacement of the interface is not known in advance and should be estimated as part of the problem. From the pioneer work of Washburn [5] on predicting the well-known displacement law, $h \sim t^{1/2}$; nowadays, the specialized literature on imbibition has been extended widely in order to take into account the influence of different factors. Recently, Alava et al. [6] presented the state of the art of imbibition in disordered media, emphasizing those aspects that have a strong influence on the interfacial description, following a statistical physics approach. Taking into account the random characteristics of disordered porous media, Alava et al. discuss the main features of imbibition: rough interfaces between both phases, fluctuations of the fluid flow, quenched noise and nonlocal effects originated from a random environment and capillary forces. Therefore, there are many possible deviations from the simple Lucas–Washburn de-

* Corresponding author. Fax: +52 55 56228106.
E-mail address: fmendez@servidor.unam.mx (F. Méndez).

0021-9797/$ – see front matter
doi:10.1016/j.jcis.2005.03.016

scription and these new fundamental studies in imbibition aid in understanding better a great variety of technological applications. Nevertheless, there is another class of imbibition processes, which under different physical conditions are only regulated by transport phenomena. Recognizing that in this direction the specialized literature is scarce, Alava et al. suggested that additional efforts are required to understanding simultaneously the imbibition and transport effects. Since the range of basic and practical aspects related to the analysis of simultaneous imbibition–transport processes is very vast, here we have focused on the theoretical study of conjugate heat transfer and imbibition in a non-Darcian porous medium. In spite of the practical importance of this class of processes, few works have appeared in the past to understand such combined effects. Phillips [7] noted that the presence of approximately uniform geothermal gradients in natural reservoirs can seriously affect the prediction of fluid dynamics. In fact, the work of Babadagli [8,9] explores the influence of a temperature field on a reservoir of oil, showing that oil production by imbibition can be controlled with the aid of a heat transfer process, injecting hot vapors. Under this situation, temperature gradients in the wetting and no-wetting phases during the imbibition process are presented. Recently, Sánchez et al. [10] developed an experimental and theoretical analysis to predict the imbibition in a Hele–Shaw cell under the influence of a uniform temperature gradient. The central result of the above work reveals that the temporal evolution of the imbibition front is sensibly affected if the surface tension and viscosity are functions of the temperature. However, the assumption of an imposed temperature gradient is too restrictive. In order to modify the previous model, we use a mathematical model which takes into account energy equations for each phase. This means that the momentum and energy equations for the wetted and dry zones must be simultaneously solved together with a equation necessary to predict the position of the imbibition front and appropriate initial and boundary conditions.

In an effort to understand the influence of imbibition on the above heat transfer process, in the present work we deal theoretically the nonisothermal imbibition of a liquid-saturated layer into a dry zone. The above process is developed in a non-Darcian porous medium, which dictates a nonlinear response. The resulting governing equations are solved numerically with a conventional finite-difference scheme. The theoretical analysis is basically organized as follows: we present a motion equation to describe the temporal evolution of the imbibition front. In contrast with other theories, the above equation is coupled to the corresponding momentum and energy equations for both phases. The above formulation includes as a particular case, the well-known Lucas–Washburn law [5] valid for isothermal imbibition. For simplicity, we assume one-dimensional flow. Afterward, we derive with the aid of an order-of-magnitude analysis the nondimensional governing equations together with the corresponding initial and boundary conditions. The resulting finite-difference equations are solved with a conventional numerical scheme. In particular, the numerical solutions show that the transient response of the imbibition front—controlled basically by the parameter β_w—substantially modifies the heat transfer process, which is also strongly affected by the presence of different nondimensional dynamics and thermal parameters introduced later.

2. Order of magnitude analysis and theoretical model

The physical model under study is shown in Fig. 1. A slender piece or sheet of height H that consists of an air-saturated porous medium (with porosity ϕ) is found initially at uniform temperature T_0 and pressure p_0. We assume thermal equilibrium between the saturated air and porous matrix. Suddenly, the lower part of the sheet touches a liquid reservoir at temperature T_1 and also with the same pressure p_0, causing an spontaneous nonisothermal imbibition of the liquid into the porous medium. This imbibition front is characterized by a uniform capillary pressure p_c. The origin of coordinates is located on the base of the sheet. We adopt a unidimensional formulation; therefore, it is enough to introduce a longitudinal or vertical coordinate y, which is measured upward in the direction of the imbibition front. The competition between thermal and dynamics penetration effects is enough to generate a nonisothermal capillary flow, which is developed inside the porous medium. We assume that the action of the gravitational acceleration is negligible. After an elapsed time t, the nonisothermal imbibition front reaches the average distance $L = L(t)$. Here, the meaning of an average distance $L(t)$ is to accept that the presence of microscopic effects is neglected in a first approximation [6]. Therefore, the presence of thermal and imbibition effects introduces two time scales: the thermal penetration scale, t_{th}, and the imbibition scale, t_i. An order of magnitude analysis makes it possible to identify both scales. For instance, applying a global energy balance for $y \geqslant 0$, the thermal energy

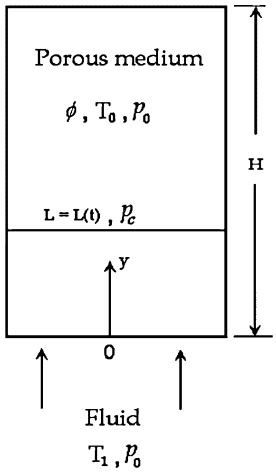

Fig. 1. Schematic view of the physical model during the nonisothermal imbibition in a porous medium.

transported by the motion of the liquid is on the same order of magnitude as the accumulation energy term. This order relationship can be written as

$$\frac{\phi\rho_w c_w U_c(T_1 - T_f)}{H} \sim \frac{(\rho c)_e(T_1 - T_f)}{t_{th}}. \tag{1}$$

In the above relationship, $(\rho c)_e$ represents the effective heat capacity of the liquid–porous matrix system. This product $(\rho c)_e$ is defined as $(\rho c)_e = \phi\rho_w c_w + (1-\phi)\rho_m c_m$, where $\rho_{w(m)}$ and $c_{w(m)}$ are the density and specific heat of the wetting liquid (or porous medium) and ϕ is the porosity of the porous matrix. Here, the subscripts w, d, and m represent wetting, drying, and porous-matrix conditions. T_f is the characteristic temperature at the imbibition front and U_c represents the characteristic volume-average velocity associated basically with the velocity of the imbibition front. This imbibition volume-average velocity is easily derived from the driven capillary pressure gradient, which dictates that $U_c \sim K(p_0 - p_c)/\phi\mu H$, where K and μ are the permeability of the porous medium and the liquid viscosity, respectively. Replacing this characteristic velocity into the relationship (1), we obtain the characteristic thermal time scale:

$$t_{th} \sim \frac{(\rho c)_e}{\rho_w c_w}\frac{\mu H^2}{K(p_0 - p_c)}. \tag{2}$$

On the other hand, the imbibition time scale is easily obtained from

$$t_i \sim \frac{H}{U_c} \sim \frac{\phi\mu H^2}{K(p_0 - p_c)}, \tag{3}$$

and combining the above relationships (1) and (2), we define the nondimensional parameter β_w as

$$\beta_w = \frac{t_{th}}{t_i} \sim \frac{(\rho c)_e}{\phi\rho_w c_w} = 1 + \frac{(1-\phi)}{\phi}\frac{\rho_m c_m}{\rho_w c_w}. \tag{4}$$

Since in conventional reservoirs $(\rho_m c_m/\rho_w c_w) \gg 1$ and the porosity ϕ can assume small values, $\beta_w \sim \rho_m c_m/\phi\rho_w c_w \gg 1$. Therefore, in order to understand the influence of the imbibition process on the transient thermal distribution in both zones, we adopt as characteristic time the thermal penetration scale t_{th}, recognizing that t_{th} is a larger scale than the t_i scale. The above permits to nondimensionalize the governing equations properly. Otherwise, if we adopt the t_i scale as characteristic time to nondimensionalize the time scale, then we would only see the initial step of the heat transfer process.

The nondimensional governing equations are presented by following the Darcy-extended Forchheimer scheme for the momentum equation, which can be found elsewhere [4], together with appropriate energy equations for wetting and dry regions. It is important to emphasize that these governing equations are derived for an incompressible Newtonian fluid flowing in an isotropic and homogeneous porous matrix. Furthermore the flow is steady, incompressible and unidimensional. Nevertheless, the existence of the porous medium introduces some additional difficulties in deriving these equations. In particular, the local thermal equilibrium, flow instabilities, momentum diffusion caused by the friction, thermal dispersion, large-scale variations in porosity, and other effects associated with the presence of the porous medium complicate the derivation of these equations. Fortunately, the above effects may be formulated using the volume average of the continuity, momentum, and energy equations [4]. Thus, introducing the nondimensional variables

$$\tau = \frac{t}{t_{th}}, \qquad \eta = \frac{y}{L(t)}, \qquad \gamma = \frac{L(t)}{H}, \qquad \zeta = \frac{y - L(t)}{H - L(t)},$$
$$u = \frac{U}{U_c}, \qquad \Phi = \frac{p - p_c}{p_0 - p_c}, \qquad \theta = \frac{T - T_0}{T_1 - T_0}, \tag{5}$$

the nondimensional governing equations can written as follows.

The mass and momentum conservation equations are

$$\frac{\partial u}{\partial \eta} = 0 \quad \text{and} \quad \frac{\partial \Phi}{\partial \eta} = -u\gamma[1 + u\mathrm{Re}_p F], \tag{6}$$

where F is the inertial coefficient, which depends on the permeability as well as the microstructure of the porous matrix [4].

The energy equation of the wetting zone is

$$\frac{\partial\theta}{\partial\tau} - \frac{\eta}{\gamma}\frac{\partial\gamma}{\partial\tau}\frac{\partial\theta}{\partial\eta} + \frac{u}{\gamma}\frac{\partial\theta}{\partial\eta} = \frac{\beta_w}{\mathrm{Pe}\gamma^2}\frac{\partial^2\theta}{\partial\eta^2}. \tag{7}$$

The energy equation of the dry zone is

$$\frac{\partial\theta}{\partial\tau} - \frac{1-\zeta}{1-\gamma}\frac{\partial\gamma}{\partial\tau}\frac{\partial\theta}{\partial\zeta} + \varepsilon\frac{u}{1-\gamma}\frac{\partial\gamma}{\partial\tau}\frac{\partial\theta}{\partial\zeta} = \frac{\alpha_{de}\beta_w}{\mathrm{Pe}(1-\gamma)^2}\frac{\partial^2\theta}{\partial\zeta^2}. \tag{8}$$

Since the position of the imbibition front, γ, is unknown, the corresponding evolution equation for the front is given by [11]

$$\gamma\frac{\partial\gamma}{\partial\tau} = -\beta_w\left.\frac{\partial\Phi}{\partial\eta}\right|_{\eta=1}, \tag{9}$$

and the initial and boundary conditions are given as

$$\gamma(\tau=0) = 0, \qquad \Phi(\eta=0) = 1, \qquad \Phi(\eta=1) = 0,$$
$$\theta(\tau=0) = 0, \qquad \theta(\eta=0) = 1, \quad \text{and} \quad \theta(\zeta=1) = 0. \tag{10}$$

Obviously, the above system of equations is solved together with the continuity of temperatures and heat transfer rates at the imbibition front:

$$\theta(\eta=1) = \theta(\zeta=0), \qquad \left.\frac{\partial\theta}{\partial\eta}\right|_{\eta=1} = \frac{k_{de}\gamma}{(1-\gamma)}\left.\frac{\partial\theta}{\partial\zeta}\right|_{\zeta=0}. \tag{11}$$

In the above equations, the nondimensional parameters Re_p and Pe represent the pore Reynolds and Peclet numbers, defined as

$$\mathrm{Re}_p = \frac{K^{1/2}U_c}{\nu} = \frac{K^{3/2}(p_0 - p_c)}{\phi\rho\nu^2 H} \quad \text{and}$$
$$\mathrm{Pe} = \frac{\phi K(p_0 - p_c)/\mu}{\alpha_e}, \tag{12}$$

and finally, the nondimensional parameters ε, k_{de}, and α_{de} are given as

$$\varepsilon = \frac{\rho_{air}c_{air}}{\rho_d c_d}\frac{(\rho c)_e}{\rho_w c_w} \ll 1, \qquad k_{de} = \frac{k_d}{k_e}, \quad \text{and} \quad \alpha_{de} = \frac{\alpha_d}{\alpha_e}. \tag{13}$$

Although $(\rho c)_e/\rho_w c_w \gg 1$, the factor $\rho_{air}c_{air}/\rho_d c_d$ is in practical cases very small, of order 10^{-5}; thus, assuming that $\varepsilon \ll 1$ is a good approach, the convective term of Eq. (8) can be neglected in a first approximation. It means that the heat convective transport in the dry region is not taking into account. Therefore, for this zone the heat transfer appears only as a transient heat conduction process. Therefore, the energy equation for the dry zone is reduced to

$$\frac{\partial\theta}{\partial\tau} - \frac{1-\zeta}{1-\gamma}\frac{\partial\gamma}{\partial\tau}\frac{\partial\theta}{\partial\zeta} = \frac{\beta_w\alpha_{de}}{\mathrm{Pe}(1-\gamma)^2}\frac{\partial^2\theta}{\partial\zeta^2}. \tag{14}$$

On the other hand, a first integration of the mass conservation equation [see Eq. (6)] dictates that $u = u(\tau)$ and recognizing also that $\gamma = \gamma(\tau)$, the corresponding momentum Eq. (6) can integrate with the boundary condition $\Phi(\eta = 0) = 1$, yielding

$$\Phi = -u\gamma[1 + u\mathrm{Re}_p F]\eta + 1. \tag{15}$$

Using the above relationship for the nondimensional pressure Φ in the nonisothermal imbibition front, we obtain a unique equation to predict the temporal evolution of γ,

$$\frac{\gamma}{\beta_w}\frac{d\gamma}{d\tau}\left(1 + \frac{\mathrm{Re}_p F}{\beta_w}\frac{d\gamma}{d\tau}\right) = 1, \tag{16}$$

subject to the initial condition $\gamma(\tau = 0) = 0$ and recognizing that $u = (1/\beta_w)(d\gamma/d\tau)$. If the product $\mathrm{Re}_p F \sim O(1)$ and $\beta_w \gg 1$ (as was previously shown); we have that $(\mathrm{Re}_p F/\beta_w) \to 0$. For this limit, we can obtain in a first approximation the Washburn law, which is easily found by integrating Eq. (16): $\gamma = (2\beta_w\tau)^{1/2}$. Therefore, we assume that for values of $(\mathrm{Re}_p F/\beta_w) \neq 0$, the corresponding imbibition fronts represent deviations of the classical Washburnian front. In this sense, we call the displacement of these fronts non-Washburnian. However, the flow patterns obey the Darcy-extended Forchheimer model. Furthermore, the energy equation, Eq. (7), in terms only of γ is reduced to

$$\frac{\partial\theta}{\partial\tau} - \frac{1}{\gamma}\frac{\partial\gamma}{\partial\tau}\frac{\partial\theta}{\partial\eta}\left(\eta - \frac{1}{\beta_w}\right) = \frac{\beta_w}{\mathrm{Pe}\gamma^2}\frac{\partial^2\theta}{\partial\eta^2}, \tag{17}$$

and Eq. (14) remains unalterable. Since the nondimensional parameter β_w, among others, defines the influence of this imbibition process on the corresponding temperature fields, which can be appreciated very well from Eqs. (14) and (17), the inverse situation is not true: the heat convection cannot determine the interface progression. Thus, the above represents a typical example of forced convection, where the flow pattern is only driven by the presence of capillary forces. The numerical scheme for the solution of the above Eq. (17), together with Eqs. (14) and (16) and the corresponding initial and boundary conditions (10) and (11) for γ and θ, is presented in the following section with particular details of the iterative numerical scheme.

3. Numerical procedure

In this section, we present the finite-differences method necessary to solve the nondimensional governing equations (14), (16), and (17) together with (10) and (11). Due to Eq. (16) being uncoupled from the energy equations, Eqs. (14) and (17), we can first integrate this equation to obtain the interfacial position of the imbibition front; i.e., $\gamma = \gamma(\tau, \mathrm{Re}_p, F, \beta_w)$ for each time step. In particular, the integration of Eq. (16) is carried out by applying the Newton–Raphson iterative method.

Introducing the above solution of γ into Eqs. (14) and (17) for the wet and the dry zones; respectively, the above equations were simultaneously solved by implementing the following iterative scheme: for a given arbitrary time τ, we assume a given value for the interface temperature, which obviously is found between $\theta_0 < \theta_i < \theta_1$. Then we calculate the temperature profile for the wetting zone, since now we dispose of two boundary conditions for the temperature and the corresponding initial condition. From this first iteration, we can also estimate the heat flux at the imbibition front and, using Eq. (11), we know the heat flux for the dry zone. The above procedure, together with the boundary condition at the top of the sheet, permits us to evaluate the temperature distribution in the dry zone. As consequence, the temperature profile and particularly the value of the temperature for the dry zone, just in the imbibition front, is compared with the above initial supposition θ_i. This process of comparison is repeated until it reaches a good convergence, guaranteeing always that temperatures and energy balance solutions in the imbibition front were carefully satisfied through of continuity conditions (11). The above iterative process is repeated to the next time $\tau + \Delta\tau$, calculating in this form the temporal evolution of the imbibition front and also the evolution of temperature profiles for both zones.

For the numerical simulation we use a range for the Peclet number between $1 \leqslant \mathrm{Pe} \leqslant 10^3$, for the parameter β_w, the range $1 \leqslant \beta_w \leqslant 150$, and a one-dimensional variable-grid size with 1000 nodes for both zones. In order to present the finite-difference equations, first we write Eq. (16) as

$$\frac{\mathrm{Re}_p F}{\beta_w}\gamma\left(\frac{d\gamma}{d\tau}\right)^2 + \gamma\frac{d\gamma}{d\tau} = \beta_w, \tag{18}$$

whose *finite-difference* version is

$$\frac{F\mathrm{Re}_p}{\beta_w}\left(\frac{\gamma_k + \gamma_{k-1}}{2}\right)\left(\frac{\gamma_k - \gamma_{k-1}}{\Delta\tau}\right)^2 + \left(\frac{\gamma_k + \gamma_{k-1}}{2}\right)\left(\frac{\gamma_k - \gamma_{k-1}}{\Delta\tau}\right) - \beta_w = 0, \tag{19}$$

and from this expression, we can obtain, after some algebraic manipulations, an implicit equation for γ_k,

$$\gamma_k = \sqrt{\gamma_{k-1}^2 + \frac{2\beta_w \Delta\tau}{\frac{F\mathrm{Re}_p}{\beta_w \Delta\tau}(\gamma_k - \gamma_{k-1}) + 1}}, \tag{20}$$

which is solved iteratively. On the other hand, the finite-difference version of Eq. (14) is written as

$$\begin{aligned}
&\theta_{i-1}^k \left\{ + \frac{(1-\bar{\gamma}^k)\frac{d\gamma^k}{d\tau}\Delta\tau}{4\Delta\zeta}(1-\zeta_i) - \frac{\beta_w \alpha_{de}\Delta\tau}{2\mathrm{Pe}\Delta\zeta^2} \right\} \\
&\quad + \theta_i^k \left\{ (1-\bar{\gamma}^k)^2 + \frac{\beta_w \alpha_{de}\Delta\tau}{\mathrm{Pe}\Delta\zeta^2} \right\} \\
&\quad + \theta_{i+1}^k \left\{ - \frac{(1-\bar{\gamma}^k)\frac{d\gamma^k}{d\tau}\Delta\tau}{4\Delta\zeta}(1-\zeta_i) - \frac{\beta_w \alpha_{de}\Delta\tau}{2\mathrm{Pe}\Delta\zeta^2} \right\} \\
&= R_i^{k-1},
\end{aligned} \tag{21}$$

together with the initial condition ($\tau = 0$) and the boundary condition (at $\zeta = 0$)

$$\theta_i^1 = 0, \qquad \theta_n^k = 0. \tag{22}$$

On the other hand, Eq. (11) is given by

$$\theta_n^k(\text{wet}) = \theta_n^k(\text{dry}) \quad \text{and}$$

$$\theta_{w,n}^k - \theta_{w,n-1}^k = \frac{k_{de}\gamma^k \Delta\eta}{(1-\gamma^k)\Delta\zeta}\left(\theta_{d,2}^k - \theta_{d,1}^k\right), \tag{23}$$

and Eq. (17) is reduced to

$$\begin{aligned}
&\theta_{i-1}^k \left\{ - \frac{\bar{\gamma}^k(\gamma^k - \gamma^{k-1})}{4\Delta\eta}\left(\frac{1}{\beta_w} - \eta_i\right) - \frac{\beta_w \Delta\tau}{2\mathrm{Pe}\Delta\eta^2} \right\} \\
&\quad + \theta_i^k \left\{ (\bar{\gamma}^k)^2 + \frac{\beta_w \Delta\tau}{\mathrm{Pe}\Delta\eta^2} \right\} \\
&\quad + \theta_{i+1}^k \left\{ + \frac{\bar{\gamma}^k(\gamma^k - \gamma^{k-1})}{4\Delta\eta}\left(\frac{1}{\beta_w} - \eta_i\right) - \frac{\beta_w \Delta\tau}{2\mathrm{Pe}\Delta\eta^2} \right\} \\
&= \bar{R}_i^{k-1},
\end{aligned} \tag{24}$$

with

$$\theta_i^1 = 0 \quad \text{and} \quad \theta_1^k = 1, \tag{25}$$

completing the final version of this finite-difference scheme. In the relationships (21) and (24), R_i^{k-1} and $\bar{R}_i^{k-1}$ represent those finite-differences terms that, being functions of the temperature, are calculated in the above time τ, $\bar{\gamma} = (\gamma_k + \gamma_{k-1})/2$, and we use the index k as superscript or subscript, indifferently.

4. Results and discussion

In all numerical calculations presented in this section, we have selected representative values of a homogeneous porous medium with an inertial coefficient $F = 0.55$, the pore Reynolds number $\mathrm{Re} = 100$ and $\alpha_{de} = 4.79 \times 10^{-3}$ [4]. The numerical results are plotted in Figs. 2–11. In these figures, we have only emphasized the importance of the nondimensional parameters Pe and β_w and should be noted that the numerical solution of Eq. (16) is independent of the temperature field; i.e., there is no influence of the temperature profiles on the flow pattern. In Fig. 2, we show the nonisothermal imbibition front γ as a function of the nondimensional time τ and three characteristic values of the nondimensional parameter β_w (= 50, 100, and 150). The influence of β_w is notable. In particular, for increasing values of this parameter, the imbibition process is strongly accelerated causing a very efficient capillary penetration. In fact, these new predictions can be better understood, following the particular temperature profiles plotted in Figs. 3–10,

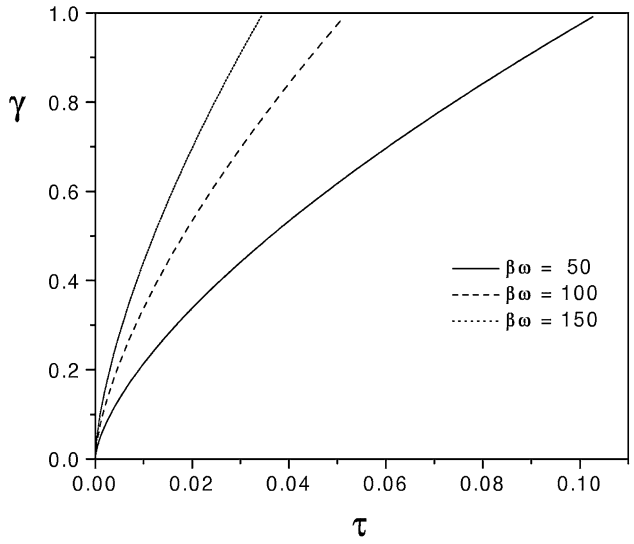

Fig. 2. Nondimensional imbibition front γ as a function of the nondimensional time τ, for three representative values of the parameter β_w (= 50, 100, and 150).

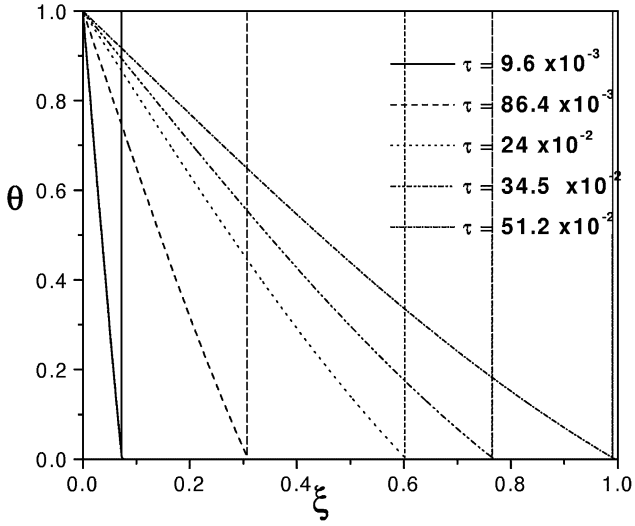

Fig. 3. Temporal evolution of the nondimensional temperature profile θ of the porous medium as a function of the nondimensional coordinate ξ for five different times, Pe = 1, and $\beta_w = 10$. Also, the imbibition front is shown for these times and is represented by vertical lines.

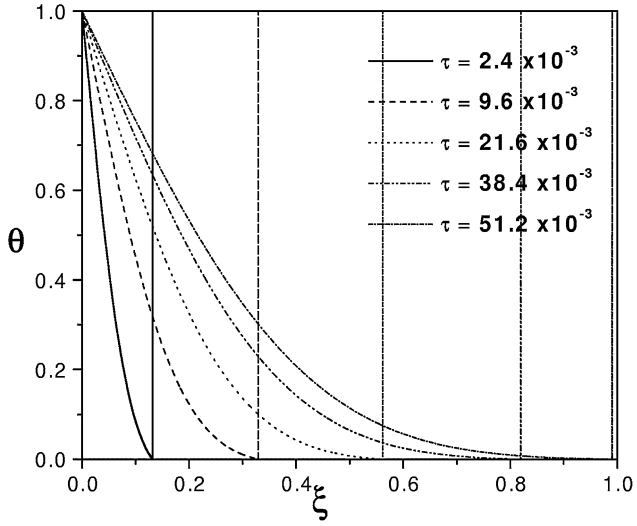

Fig. 4. Temporal evolution of the nondimensional temperature profile θ of the porous medium as a function of the nondimensional coordinate ξ for five different times, Pe = 1, and $\beta_w = 100$. Also, the imbibition front is shown for these times and is represented by vertical lines.

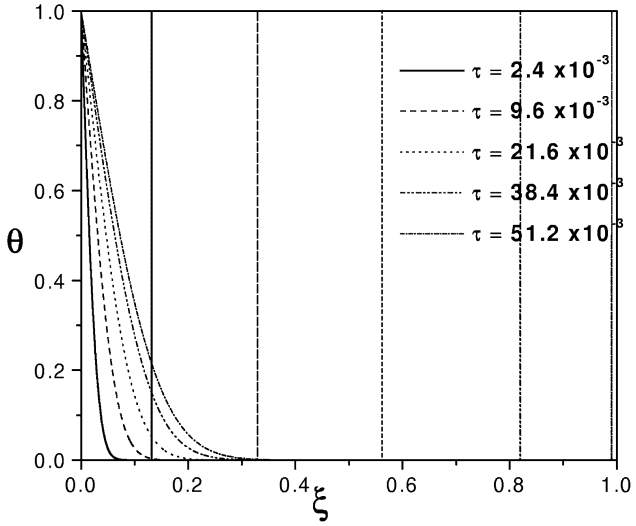

Fig. 6. Temporal evolution of the nondimensional temperature profile θ of the porous medium as a function of the nondimensional coordinate ξ for five different times, Pe = 10, and $\beta_w = 100$. Also, the imbibition front is shown for these times and is represented by vertical lines.

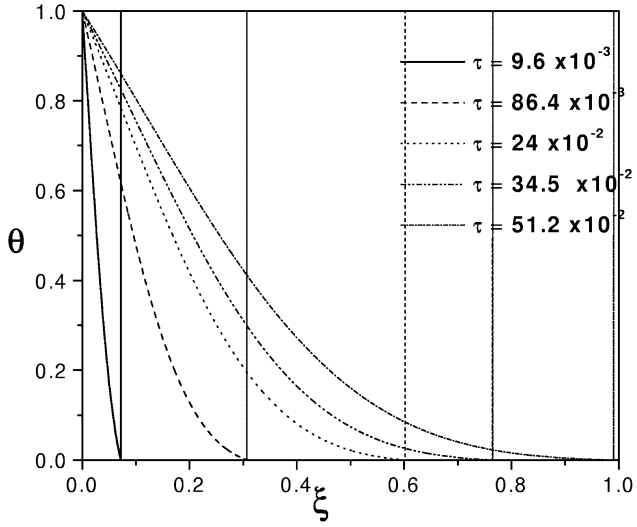

Fig. 5. Temporal evolution of the nondimensional temperature profile θ of the porous medium as a function of the nondimensional coordinate ξ for five different times, Pe = 10, and $\beta_w = 10$. Also, the imbibition front is shown for these times and is represented by vertical lines.

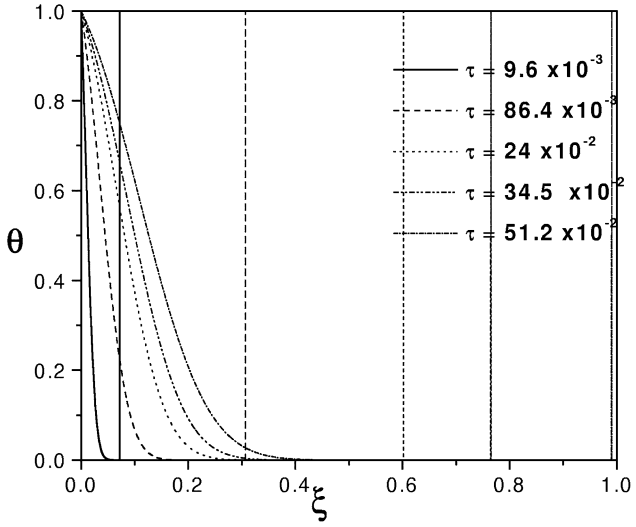

Fig. 7. Temporal evolution of the nondimensional temperature profile θ of the porous medium as a function of the nondimensional coordinate ξ for five different times, Pe = 100, and $\beta_w = 10$. Also, the imbibition front is shown for these times and is represented by vertical lines.

including for different times the imbibition fronts. Accordingly, we present in these figures for different values of Pe and β_w, the temporal evolution of the nondimensional temperature profile, θ, as a function of the nondimensional coordinate $\xi = y/H$. We use ξ because in terms of this variable, the complete domain of interest is shown (wetting and dry zones). Also, in these figures, the vertical lines represent the position of the imbibition front for different values of the nondimensional time τ. In Fig. 3 with Pe = 1 and $\beta_w = 10$, the results show quasi-linear behavior of the temperature for the wetting zone and just in the imbibition front, the temperature reaches the values of $\theta \approx 0$, independent of the position of the front. The above indicates that the dry zone is found totally in thermal equilibrium with temperature $\theta = 0$. Then, we can visualize this result as a slow regime that permits that the front reaches the thermal equilibrium with dry zone. In Fig. 4, a similar behavior is obtained for Pe = 1 and $\beta_w = 100$; however, when we increase the value of β_w, the convective transport of the thermal energy is strongly accelerated, causing also a quicker displacement of the front, which can be appreciated very well by comparing Figs. 3 and 4 for equal times. In Figs. 5 and 6, we increase the Peclet number to understand its influence. In Fig. 5, for Pe = 10 and $\beta_w = 10$, the temperature profile is attenuated in comparison with Fig. 3, because the fronts in both figures occupied the same positions. Therefore, increasing Peclet numbers is

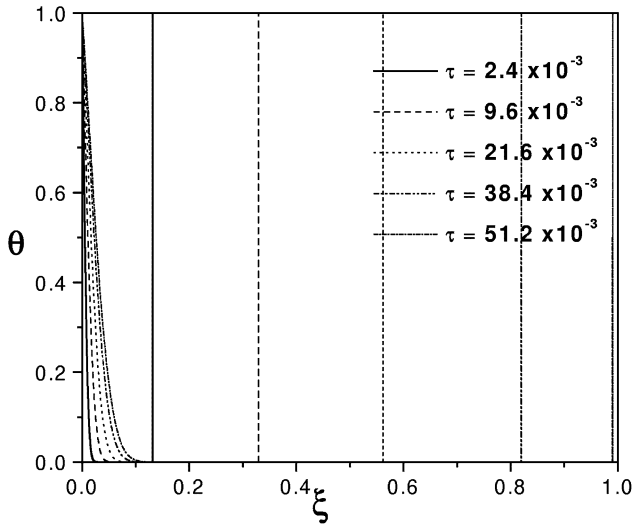

Fig. 8. Temporal evolution of the nondimensional temperature profile θ of the porous medium as a function of the nondimensional coordinate ξ for five different times, Pe = 100, and $\beta_w = 100$. Also, the imbibition front is shown for these times and is represented by vertical lines.

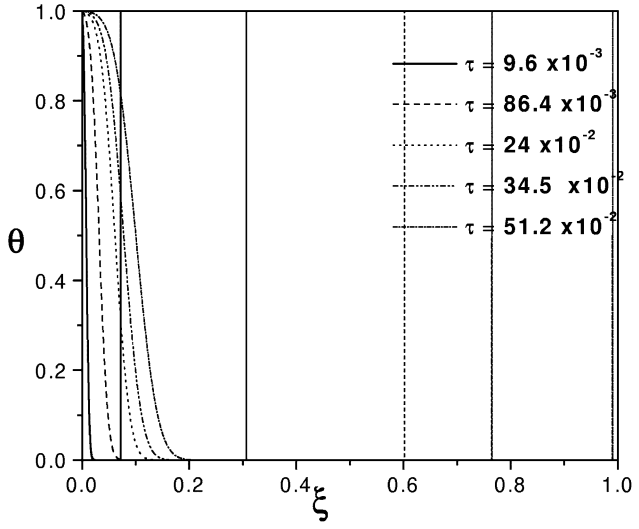

Fig. 9. Temporal evolution of the nondimensional temperature profile θ of the porous medium as a function of the nondimensional coordinate ξ for five different times, Pe = 1000, and $\beta_w = 10$. Also, the imbibition front is shown for these times and is represented by vertical lines.

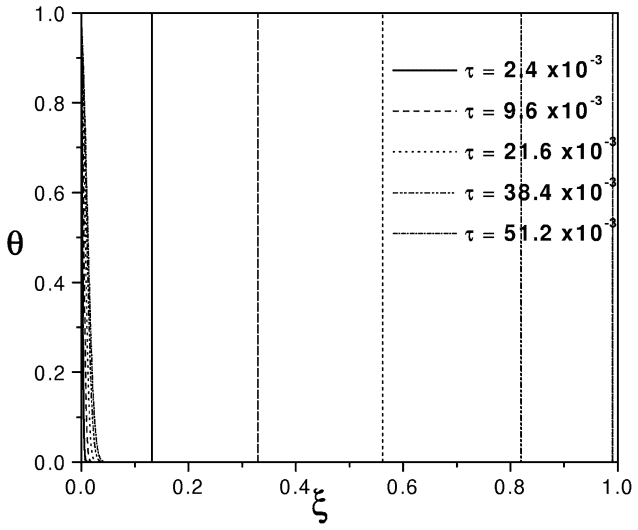

Fig. 10. Temporal evolution of the nondimensional temperature profile θ of the porous medium as a function of the nondimensional coordinate ξ for five different times, Pe = 1000, and $\beta_w = 100$. Also, the imbibition front is shown for these times and is represented by vertical lines.

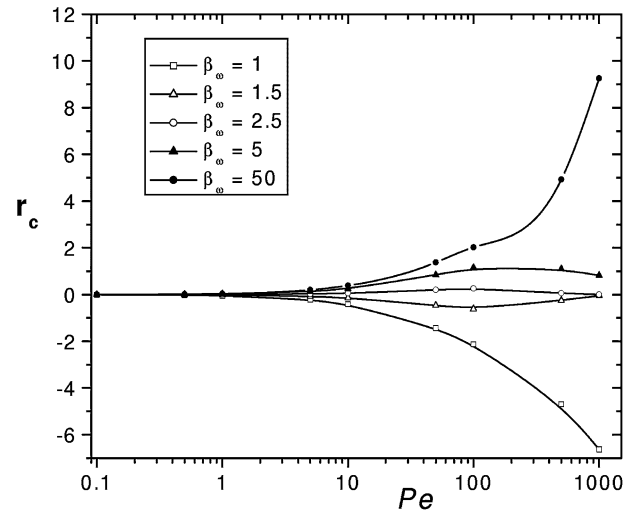

Fig. 11. Average radius of curvature of the temperature, r_c, as a function of the Peclet number, Pe, and five different values of the nondimensional parameter β_w (= 1, 1.5, 2.5, 5, and 50).

equivalent to reducing the transport of thermal energy. The above is drastically amplified with Pe = 10 and $\beta_w = 100$ as is illustrated in Fig. 6. In this case, the displacement of the front is vigorous; however, the convective transport of the thermal energy is not as efficient as in above figures. In particular for this last figure, the thermal equilibrium is reached in the wetting zone, because for increasing values of the time, the imbibition front advances with $\theta = 0$. This behavior is more pronounced yet in Figs. 7–10, showing clearly a boundary layer structure for temperature profiles. For instance, if Fig. 7 with Pe = 100 and $\beta_w = 10$ is compared with Fig. 5, because both have the same value of the parameter β_w, the thermal boundary layer is thinner for Fig. 7. It is obtained the same result comparing Figs. 6 and 8 with $\beta_w = 100$ and Pe = 10 and 100, respectively. For very large values of Peclet, Figs. 9 and 10 complement these results. Comparing both figures for Pe = 1000, can easily see that for increasing values of β_w, again, the thermal boundary layer is more pronounced.

Finally, in Fig. 11 we have plotted the following phase diagram: the average radius of curvature of the temperature field as a function of the Peclet number, five different values of the parameter β_w (= 1, 1.5, 2.5, 5, and 50), $F = 0.55$, Re = 100, and $\alpha_{de} = 4.79 \times 10^{-3}$. Here, the average radius

of curvature, r_c, is defined as

$$r_c = \frac{\overline{\partial^2\theta}}{\partial\xi^2} = \frac{\int_0^1 \frac{\partial^2\theta}{\partial\xi^2}\big|_{\gamma=1/2}\,d\xi}{\int_0^1 d\xi},$$

and the subscript on the second derivative of θ in the above definition represents the value of this derivative when the front position is $\gamma = 1/2$. This means that for each value of the parameter β_w, we reach the front position $\gamma = 1/2$ for a specific time. Obviously, this value of the front was arbitrarily choose. However, we have not found in figures similar to Fig. 11 with other values of γ a very different behavior. Therefore, there is practically a critical value of the parameter $\beta_w = \beta_{wcr} \sim 2$, for which the average radius of curvature changes of sign from negative to positive, indicating indeed that this parameter serves to define the concavity of the temperature profiles.

5. Summary

In this work the problem of nonisothermal imbibition under a sudden temperature step in a non-Darcian porous medium has been numerically analyzed through the use of a motion equation for the imbibition front coupled with the corresponding energy equations for the wetting and dry zones. The requirement to introduce these energy balance equations comes from the fact that the temperature at the imbibition front is unknown, transforming this nonisothermal imbibition process into a conjugate heat transfer analysis. To our knowledge, the present model has not been previously reported in the specialized literature, although this class of processes is physically important in water and oil reservoirs.

Acknowledgments

This work was supported by the following grants: SAB2002-0137 of the Ministerio de Educación, Cultura y Deporte of Spain and 43010-Y from CONACyT at Mexico. M. Sánchez also acknowledges the “Programa de Estancias de Entrenamiento en Yacimientos, Instituto Mexicano del Petróleo.”

References

[1] V.G. Levich, Physicochemical Hydrodynamics, Prentice–Hall, Englewood Cliffs, NJ, 1962.
[2] S. Middleman, Modeling Axisymmetric Flows, Academic Press, New York, 1995.
[3] C. Isenberg, The Science of Soap Films and Soap Bubbles, Dover, New York, 1992.
[4] K. Vafai, Handbook of Porous Media, Dekker, New York, 2000.
[5] E.W. Washburn, Phys. Rev. 17 (1921) 273.
[6] M. Alava, M. Dubé, M. Rost, Adv. Phys. 53 (2004) 83.
[7] O.M. Phillips, Flow and Reactions in Permeable Rocks, Cambridge Univ. Press, Cambridge, UK, 1991.
[8] T. Babadagli, J. Pet. Sci. Eng. 14 (1996) 197.
[9] T. Babadagli, J. Pet. Sci. Eng. 33 (2002) 223.
[10] M. Sánchez, F. Sánchez, C. Pérez-Rosales, A. Medina, C. Treviño, Phys. Lett. A 324 (2004) 14.
[11] J.A. Liggett, P.L.-F. Liu, The Boundary Integral Equation Method for Porous Media Flow, George Allen, London, 1983.